

RESEARCH ARTICLE

Role of Structural Dynamics at the Receptor G Protein Interface for Signal Transduction

Alexander S. Rose^{1,2}, Ulrich Zachariae^{5,6}, Helmut Grubmüller⁵, Klaus Peter Hofmann^{1,4}, Patrick Scheerer^{1,3}, Peter W. Hildebrand^{1,2*}

1 Institute of Medical Physics and Biophysics (CC2), Universitätsmedizin Berlin, Charitéplatz 1, 10098, Berlin, Germany, **2** Team Proteoinformatics, Universitätsmedizin Berlin, Charitéplatz 1, 10098, Berlin, Germany, **3** Team Protein X-ray Crystallography and Signal Transduction, Charité - Universitätsmedizin Berlin, Charitéplatz 1, 10098, Berlin, Germany, **4** Centre of Biophysics and Bioinformatics, Humboldt-Universität zu Berlin, Invalidenstrasse 42, 10115, Berlin, Germany, **5** Dep. of Theoretical and Computational Biophysics, Max-Planck-Institute for Biophysical Chemistry, 37077, Göttingen, Germany, **6** Computational Biology, School of Life Sciences, and Physics, School of Science and Engineering, University of Dundee, Dow Street, Dundee, DD1 5EH, United Kingdom

* peter.hildebrand@charite.de



OPEN ACCESS

Citation: Rose AS, Zachariae U, Grubmüller H, Hofmann KP, Scheerer P, Hildebrand PW (2015) Role of Structural Dynamics at the Receptor G Protein Interface for Signal Transduction. PLoS ONE 10(11): e0143399. doi:10.1371/journal.pone.0143399

Editor: Eugene A. Permyakov, Russian Academy of Sciences, Institute for Biological Instrumentation, RUSSIAN FEDERATION

Received: August 17, 2015

Accepted: November 4, 2015

Published: November 25, 2015

Copyright: © 2015 Rose et al. This is an open access article distributed under the terms of the [Creative Commons Attribution License](https://creativecommons.org/licenses/by/4.0/), which permits unrestricted use, distribution, and reproduction in any medium, provided the original author and source are credited.

Data Availability Statement: All relevant data are within the paper and its Supporting Information files.

Funding: This work was supported by the Deutsche Forschungsgemeinschaft Sfb740 (to K.P.H., P.S. and P.W.H.), Sfb1078-B6 (to P.S.), DFG HI 1502/1-1 (to P.W.H.), BI 893/8 (to P.W.H.), DFG Cluster of Excellence 'Unifying Concepts in Catalysis' (Research Field D3/E3-1 to P.S.) and ERC Advanced grant (ERC-2009/249910—TUDOR to K.P.H.). The computer time necessary for this project was provided in part by the "Norddeutscher Verbund für Hoch und Höchstleistungsrechner" (HLRN). U.Z.

Abstract

GPCRs catalyze GDP/GTP exchange in the α -subunit of heterotrimeric G proteins ($G\alpha\beta\gamma$) through displacement of the $G\alpha$ C-terminal $\alpha 5$ helix, which directly connects the interface of the active receptor (R^*) to the nucleotide binding pocket of G. Hydrogen–deuterium exchange mass spectrometry and kinetic analysis of R^* catalysed G protein activation have suggested that displacement of $\alpha 5$ starts from an intermediate GDP bound complex ($R^*\bullet G^{GDP}$). To elucidate the structural basis of receptor-catalysed displacement of $\alpha 5$, we modelled the structure of $R^*\bullet G^{GDP}$. A flexible docking protocol yielded an intermediate $R^*\bullet G^{GDP}$ complex, with a similar overall arrangement as in the X-ray structure of the nucleotide free complex ($R^*\bullet G^{empty}$), however with the $\alpha 5$ C-terminus ($G\alpha CT$) forming different polar contacts with R^* . Starting molecular dynamics simulations of $G\alpha CT$ bound to R^* in the intermediate position, we observe a screw-like motion, which restores the specific interactions of $\alpha 5$ with R^* in $R^*\bullet G^{empty}$. The observed rotation of $\alpha 5$ by 60° is in line with experimental data. Reformation of hydrogen bonds, water expulsion and formation of hydrophobic interactions are driving forces of the $\alpha 5$ displacement. We conclude that the identified interactions between R^* and G protein define a structural framework in which the $\alpha 5$ displacement promotes direct transmission of the signal from R^* to the GDP binding pocket.

Introduction

G protein coupled receptors (GPCRs) transmit extracellular signals into the cell through binding of heterotrimeric G proteins ($G\alpha\beta\gamma$, classified as G_i , G_t , G_s , . . .) and catalysing GDP/GTP exchange in the $G\alpha$ subunit ([Fig 1](#)). Detailed insights into the structural changes triggering GDP release were obtained from recent X-ray structures of inactive (R) and active receptor

acknowledges funding from the Scottish Universities Physics Alliance and the UK National Physical Laboratory. The funders had no role in study design, data collection and analysis, decision to publish, or preparation of the manuscript.

Competing Interests: The authors have declared that no competing interests exist.

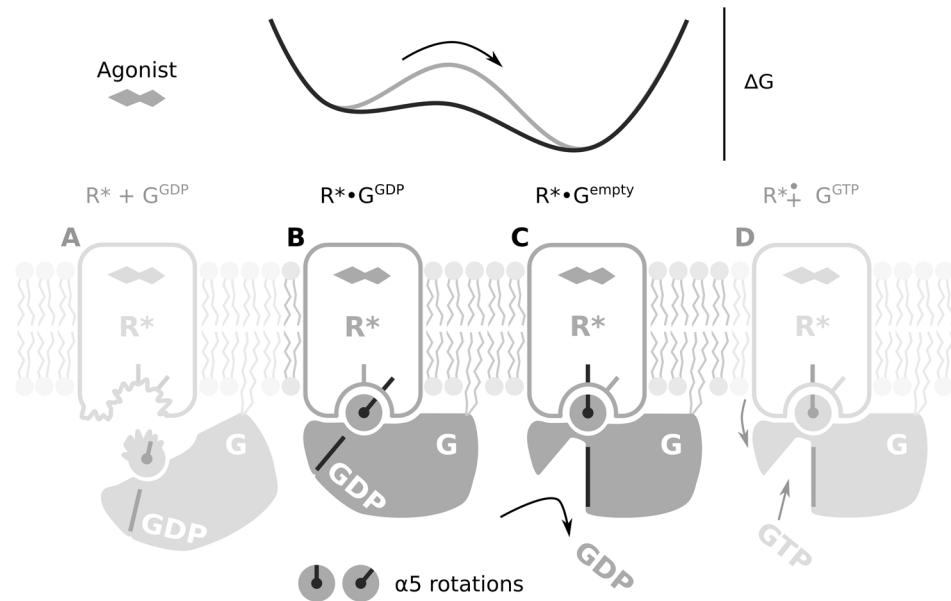


Fig 1. Role of the $\alpha 5$ helix in the interaction between R^* and G that leads to nucleotide exchange. From left to right. (A) Membrane anchored G^{GDP} with an unstructured $\alpha 5$ C-terminus encounters R^* with a partially unstructured cytoplasmic crevice. (B) The intermediate $R^* \cdot G^{GDP}$ complex is formed through mutual structuring of the $\alpha 5$ C-terminus and the R^* cytoplasmic crevice. The $\alpha 5$ helix has not yet rotated compared to unbound G^{GDP} . (C) Rotation of $\alpha 5$ lowers the energy barrier separating $R^* \cdot G^{GDP}$ from nucleotide free $R^* \cdot G^{empty}$ resulting in GDP release. (D) Uptake of GTP and dissociation of G^{GTP} completes the nucleotide exchange reaction.

doi:10.1371/journal.pone.0143399.g001

states (R^*) [1], of GDP bound G proteins (G^{GDP}) and the nucleotide free $R^* \cdot G$ complex ($R^* \cdot G^{empty}$) [2,3]. A rearrangement within the 7-transmembrane helix (7-TM) bundle opens a cytoplasmic crevice in R^* for binding of G^{GDP} [1,3–6]. In unbound G^{GDP} , the nucleotide is tightly bound by the $G\alpha$ helical and Ras domain enveloping the nucleotide [7]. In the $R^* \cdot G^{empty}$ complex, the Ras domain $\alpha 5$ helix ($\alpha 5$) and the helical domain of $G\alpha$ are displaced and the nucleotide pocket is emptied (Fig 1C). The $\alpha 5$ helix, which forms a direct linkage between the cytoplasmic R^* crevice and the nucleotide free binding pocket, is considered the principal structural element in transmission of the signal from R^* to the nucleotide binding pocket [8–10]. The mechanism by which R^* triggers the displacement of $\alpha 5$ is thus key to understanding the catalytic function of GPCRs.

New insights into the structural basis for nucleotide exchange came from recent multi-microsecond MD simulations and DEER measurements [10]. These experiments show that displacement of the helical domain occurs spontaneously without GDP release in G^{GDP} even in the absence of R^* . However, $\alpha 5$ is spontaneously only displaced when GDP has been omitted, or when the effect of R^* is mimicked by restraining $\alpha 5$ in the $R^* \cdot G^{empty}$ position. These observations corroborate the important role of $\alpha 5$ for signal transmission. The key question of the mechanism of $\alpha 5$ displacement by R^* , and the course of events leading to GDP release, however, still remains to be elucidated.

Simulation of the complete process of receptor G protein association and catalysis of GDP/GTP exchange takes milliseconds and is thus presently still beyond computationally accessible time scales [10–12]. However, the characterisation of structural intermediates and simulations of intermediate steps are promising approaches to obtain insights into the structural mechanism of R^* catalysed nucleotide exchange. Here, we focus on the $R^* \cdot G^{GDP}$ intermediate

complex (Fig 1B), which is visited during the progression from R^* and G^{GDP} (Fig 1A) to the $R^* \cdot G^{empty}$ complex (Fig 1C). Evidence for the $R^* \cdot G^{GDP}$ complex, in which both the receptor and GDP are bound to the G protein, has been found in the kinetics of Gt activation in rod disc membranes [13,14] and in hydrogen—deuterium exchange mass spectrometry (HDX) data of Gs activation by the activated β_2 adrenoceptor (β_2AR^*) [15]. Formation of $R^* \cdot G^{GDP}$ pre-complexes seems to affect the specificity and kinetics of signal transmission [16,17] and may also play an important mechanistic role in R^* catalysed signal transfer. In this study, we present a computational investigation of the structure and function of the $R^* \cdot G^{GDP}$ complex, which has not been resolved by protein X-ray crystallography. We will focus on the question how this complex relates to the displacement of $\alpha 5$ upon G protein activation, which we have previously termed $\alpha 5$ helix-switch [14] (Fig 1B and 1C).

Upon binding to $R^{3.50}$ within the conserved D[E]RY motif at the floor of the cytoplasmic crevice of R^* , the far C-terminus of $\alpha 5$ (termed $G\alpha CT$) adopts the structure of a continuous α -helix capped by a C-terminal reverse turn [3,5,18–22]. FTIR spectroscopy and MD simulations have elucidated the mutual structuring of the involved binding interfaces (indicated in Fig 1A–1C) [18,23–25]. Recent atomic-level simulations show that the structured conformation of $G\alpha CT$ can also occur in absence of R^* [10]. In HDX experiments of Gs activation by the β_2AR^* ($\beta_2AR^* \cdot Gs$), deuterium exchange rates increase only slightly at the Gs $\alpha 5$ C-terminus ($Gs\alpha CT$) after adding GDP to the nucleotide free preparation, and the low exchange rates indicate structured elements. In contrast, adding the non-hydrolyzable GTP analog GTP γ S uncouples Gs from $\beta_2AR^* \cdot Gs^{empty}$ and results in high exchange rates of $Gs\alpha CT$ [15]. These data suggest that in the $\beta_2AR^* \cdot Gs^{GDP}$ intermediate complex, $Gs\alpha CT$ already adopts a helical conformation, stabilized by interactions with β_2AR^* . The HDX experiments have also indicated that, on the N-terminal end of $\alpha 5$, the contacts that stabilize GDP in its binding pocket are preserved in the $\beta_2AR^* \cdot Gs^{GDP}$ intermediate. Summarizing these measurements, it seems reasonable that in $R^* \cdot G^{GDP}$ $\alpha 5$ is not yet displaced and that the overall topology of the Ras domain of G^{GDP} is preserved. Alignment of $G\alpha^{GDP}$ with X-ray structures representing nucleotide free complexes, however, results in major clashes of $G\alpha^{GDP}$ with R^* and the membrane (see e.g. Fig 5 of ref. [5] or Fig S13 of ref. [10]). Thus, $\alpha 5$ must bind with a different orientation to R^* in the GDP bound compared to the nucleotide free complex to produce a clash free arrangement.

The present investigation was motivated by our previous finding [14] that flexible docking of $Gt\alpha CT$ 15- and 19-mer peptides to active rhodopsin (RhR^*) yielded two different poses. The first pose recovered the topology of the $RhR^* \cdot Gt\alpha CT$ X-ray structure (i.e. the most likely position of $\alpha 5$ in $R^* \cdot Gi/t^{empty}$ [25,26]). Alignment of G^{GDP} to a second pose of $Gt\alpha CT$ resulted in a clash free complex with RhR^* , which we assigned to the intermediate $RhR^* \cdot Gt^{GDP}$ complex [14]. In the present analysis of Gs^{GDP} binding to β_2AR^* , we applied the same docking protocol to $Gs\alpha CT$ and β_2AR^* . We again detect one pose, which recovers the topology of $\beta_2AR^* \cdot Gs^{empty}$ and a second pose yielding $\beta_2AR^* \cdot G^{GDP}$. Both models of $\beta_2AR^* \cdot G^{GDP}$ and $RhR^* \cdot G^{GDP}$ closely resemble the overall arrangement of the $R^* \cdot G^{empty}$ complex, except that $\alpha 5$ forms distinct interactions with R^* . The main change in the interactions of GDP bound and empty complexes triggers a rotation of $\alpha 5$ by about 60° within the cytoplasmic crevice of R^* , which is exactly the value by which $\alpha 5$ is displaced during activation [9,26]. Our model suggests that the $\alpha 5$ displacement occurs within a fixed structural framework defined by the interactions between intracellular loop 2 (ICL2) of R^* and structural elements of the G protein. To study the role of R^* for the displacement of $\alpha 5$, we conducted MD simulations of $Gs\alpha CT$ and $Gt\alpha CT$ in the cytoplasmic crevices of β_2AR^* and RhR^* , respectively, from our intermediate $R^* \cdot G^{GDP}$ complexes. Reformation of hydrogen bonds, water expulsion and formation of hydrophobic interactions are found as the forces that drive the characteristic displacement of $\alpha 5$ within the cytoplasmic crevice of R^* .

Results

A docking pose of a G α CT peptide that belongs to the β_2 AR*•G^{GDP} complex

The first goal of this study was to model the GDP bound intermediate β_2 AR*•G^{GDP} complex that is visited in the progression from β_2 AR* and G^{GDP} to the R*•G^{empty} complex. Structural intermediates generally form towards the end of the protein association pathway after the rate-limiting step [27], which in case of the fast signal transfer from receptors to G proteins involve folding of G α CT and ICL3 [18,24]. We therefore applied flexible docking with fixed α -helical backbone geometry but flexible side chains of a 15-mer G α CT peptide to the cytoplasmic crevice of β_2 AR* (Protocol C in S1 File). The coordinates of both the peptide and the receptor were extracted from the X-ray structure of the β_2 AR*•G^{empty} complex.

As in our previous analysis of G α CT docking to RhR* [14], the highest scored docking pose of 15-mer G α CT to β_2 AR* confirms the position and orientation seen in the X-ray structure of the nucleotide free complex (Fig G in S1 File; first cluster: 11 of 110 poses). In this pose, the characteristic cation- π interaction observed in β_2 AR*•G^{empty} is formed between Y391 of the C-terminal cap of G α CT to R131^{3.50} of β_2 AR* (Fig 2B). Moreover, specific contacts are formed between the N-terminus of G α CT with ICL2 and ICL3 of β_2 AR* (Fig 2D). These contacts involve potential hydrogen bonds of Q384 of G α CT with the main chain carbonyl group of I135^{3.54} from the conserved P138^{3.57} helix cap motif (Table A of S1 File), which terminates TM3 of β_2 AR*. In a second docking pose (Fig G of S1 File; third cluster: 6 of 110 poses) the contact of G α CT with R131^{3.50} is shifted C-terminally by one residue from Y391 to E392 (Fig 2A and 2B). N-terminally, the contact of G α CT with the main chain carbonyl group of I135^{3.54} is also shifted by one residue from Q384 to R385 (Fig 2C and 2D; Table A of S1 File). We thus obtain not only the pose of G α CT displayed by the X-ray structure (which validates the applicability of the docking approach) but also a second pose, in which G α CT is rotated around its axis.

In the two poses, G α CT binds to the same conserved structural motifs of β_2 AR*, however via different residues. Comparison of the two poses reveals that the shift of the interacting residues by one position entails a rotation of G α CT by 60° and a translation by 1.5 Å (see Protocol E in S1 File). Of note, a similar rotation has also been observed when the two poses obtained from flexible docking of G α CT to RhR* were compared [14]. Since G α 5 undergoes a rotation of the same magnitude during G protein activation (Fig F in S1 File), superposition of nucleotide bound states of G α ^{GTP γ S} (PDB entry 1AZT) or G^{GDP} (PDB entry 1GOT) with G α CT of that second pose creates a complex with a very similar overall arrangement as in β_2 AR*•G^{empty}, but in which α 5 is rotated by 60° (Fig 2E and 2F). As in our previous analysis of the RhR* interaction with G^{GDP}, this new state does not cause any major protein-protein/protein-membrane clashes or distortions. Since α 5 is also structured and G^{GDP} is not altered in that complex (see Fig 2E), it is assigned to the β_2 AR*•G^{GDP} complex. As a result of our docking analysis, we predict that the α 5 helix-switch is triggered through sequential interactions of α 5 with the cytoplasmic crevice of R*.

Observation of helix-switches by molecular dynamics simulations

To evaluate the forces which guide the α 5 helix-switch from the GDP bound to the nucleotide free state, we started MD simulations from the intermediate β_2 AR*•G α CT and RhR*•G α CT complexes. Using the R*•G α CT complexes ensures that only the interactions of G α CT with R*, but not of α 5 with the remainder of the G holo protein play a role. Most simulations were performed with 11-mer G α CT peptides, as it is the largest common structure in the available

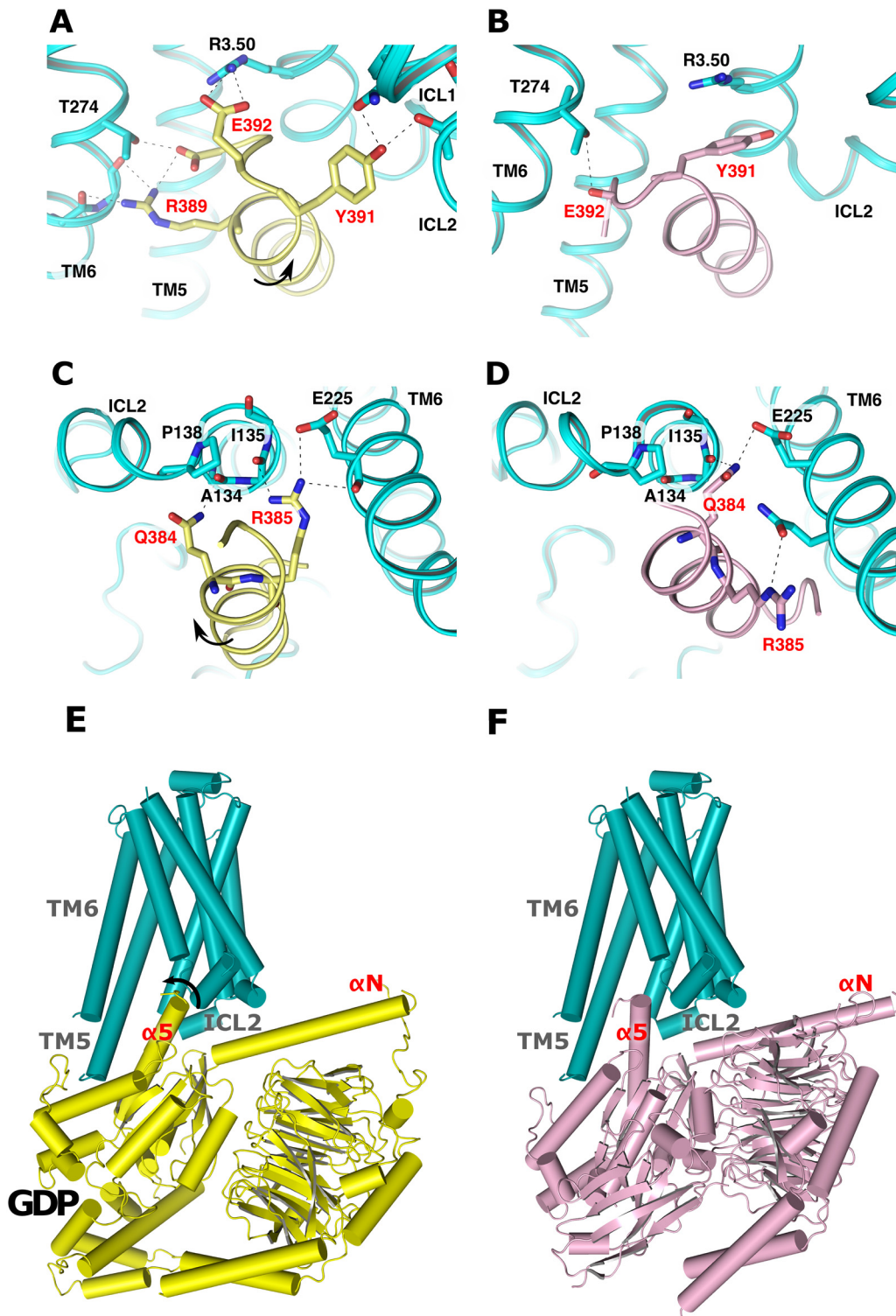


Fig 2. Comparison of the $\beta_2AR^*Gs^{GDP}$ model (left panel) and the $\beta_2AR^*Gs^{empty}$ X-ray structure (right panel). The figure illustrates potential hydrogen bonds to residues within the cytoplasmic crevice (cyan cartoon) from (A, B) the C-terminal reverse turn and (C, D) the N-terminus of GsaCT. (A, C) shows the intermediate position obtained from flexible docking of 15-mer GsaCT (yellow cartoon) and (B, D) the position in the nucleotide free complex (magenta cartoon), respectively. Residue labels from β_2AR^* are colored in black, from GsaCT in red. Potential hydrogen bonds are denoted as black dashed lines. (E) Complete model of the $\beta_2AR^*Gs^{GDP}$ intermediate compared to (F) the $\beta_2AR^*Gs^{empty}$ X-ray structure (PDB entry 3SN6). R^*G^{GDP} was obtained by superposition of $Gsa^{GTP_{PYS}}$ (PDB entry 1AZT) with the intermediate $\beta_2AR^*Gs^{GDP}$ complex by common backbone atoms. Black arrows indicate the rotation of $\alpha 5$.

doi:10.1371/journal.pone.0143399.g002

experimental data [3,5,18]. To evaluate the effect of peptide length, we performed additional simulations with 19-mer G α CT peptides, in total 4 simulations for β_2 AR*•G α CT and 6 for RhR*•G α CT. During all MD simulations, G α CT was neither restricted to its starting conformation nor in its mobility.

From the total of 60 MD simulations of 11-mer G α CT, 30*200 ns for the β_2 AR* and 30*100 ns for RhR* systems, 18 feature a helix-switch, 8 for G α CT and 10 for G α CT. In these simulations, the 11-mer adopts a conformation maintained for the remainder of the simulation (Figs N, O, P, Q and R in [S1 File](#)). These 'stable' binding modes form quickly, within 50 ns in case of G α CT and within 3 ns in case of 11-mer G α CT. In these simulations we observe a switch-like transition to the position seen in the corresponding X-ray structures. The different time scales observed for the transitions likely originate from the different properties of the corresponding binding interfaces. The larger interface of 11-mer G α CT with the β_2 AR* (62.7 Å²) as of G α CT with RhR* (35.9 Å²) in the intermediate, presumably slows down the switch motion. This relatively small difference of about 50 ns may not be relevant for the holo G protein, where additional contacts of $\alpha 5$ with G^{GDP} slow down the $\alpha 5$ helix-switch to the microsecond scale [10]. All transitions were monitored by the parameters peptide backbone-RMSD ([Fig 3A and 3B](#) and [Fig N](#) in [S1 File](#)) and peptide rotation ([Fig 3C and 3D](#) and [Fig N](#) in [S1 File](#)).

Despite the fact that two different receptors and peptides were simulated, the two G α CT peptides undergo similar screw-like motions to re-establish the key interactions with R^{3.50} seen in the respective X-ray structures. Formation of these latter interactions, which belong to the nucleotide free state, becomes apparent in the time resolved analyses of distance and energy ([Fig 3E and 3F](#), [Fig O](#) in [S1 File](#)). Whilst the secondary structure of G α CT remains stable ([Fig P](#) in [S1 File](#)), a significant number of water molecules are displaced from the binding interface in favour of a hydrophobic patch that is formed between G α CT and ICL3 of R* (Figs K, Q and R in [S1 File](#)). The water molecules that remain bound to the interface in the MD simulation coincide with water molecules resolved in X-ray structures of RhR*•G α CT ([Fig S](#) in [S1 File](#)). In the simulations in which no stable binding mode is observed, G α CT fluctuates between different orientations and positions, diffuses away and unfolds. Only one additional stable binding mode of G α CT is obtained in simulations 11 and 12 (Panel B of Figs N, O, P, Q and R in [S1 File](#)). In these simulations, G α CT is tilted steeper by 10° relative to the membrane plane compared to those in which a complete switch event is observed.

The simulations of 19-mer G α CT show a similar result to the 11-mer peptides (Panels B and C of [Fig J](#) in [S1 File](#)). Two helix-switch events were observed for each of the systems (RhR* and β_2 AR*) after about 50 ns of 200–400 ns simulation time, respectively, accounting for more than one third of the simulations. Presumably due to the lack of stabilizing contacts with R*, the first N-terminal turn of 19-mer G α CT undergoes helix-coil transitions during the switch (Panel A of [Fig J](#) in [S1 File](#)). By contrast, the secondary structure of the C-terminal reverse turn of switched G α CT is preserved and essentially immobilized through interactions with R* (grey bars in [Fig 3A, 3C and 3E](#)).

Discussion

Characterisation of the R*•G^{GDP} intermediate

Protein-protein interactions follow a multi-state process, from an initial encounter through an intermediate to the final functional complex [27]. Intermediates are thus envisioned as pre-formed complexes whose reorganization leads to the final functional complex. They form towards the end of the protein association pathway after the rate-limiting step, which in case of the fast signal transfer from receptors to G proteins involve a stepwise and mutual reduction of the conformational space of G α CT and ICL3 [18,24]. Set after the rate limiting step, the C-

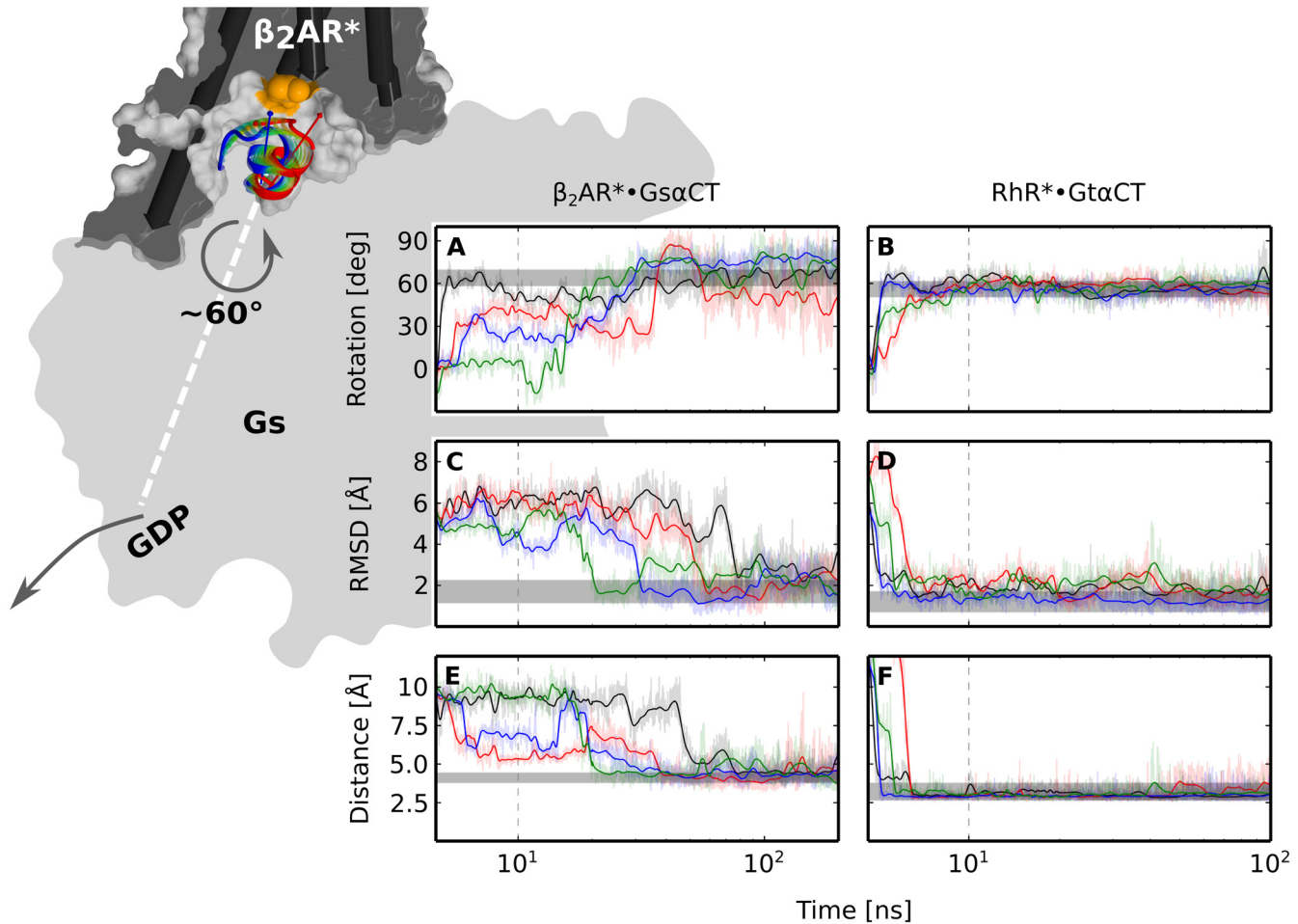


Fig 3. Switch of GsaCT (left) and GtaCT (right) at the R* interface observed in MD simulations. Background figure: GsaCT switches within the cytoplasmic crevice of β_2AR^* from the intermediate (red) to the nucleotide free position (blue). The transition is schematically indicated by semi-transparent colored cartoons. GsaCT is rotated around its helix axis (red and blue arrows) by about 60° , which eventually triggers GDP release from the nucleotide binding pocket of the Gs holoprotein (gray, flat shaded). In addition a tilt motion of GsaCT parallel to the membrane plane is observed. The surface of the receptor (gray) is cut at the position of R^{3.50} (orange patch) located at the floor of the cytoplasmic crevice. TM helices are shown as cylinders. For clarity, H8 and H6 of β_2AR^* are omitted. The panel in the foreground shows rotation of (A) GsaCT or (B) GtaCT around its helix axis; backbone-RMSD of (C) GsaCT or (D) GtaCT relative to the position in the X-ray structure; distance between (E) the center of the phenyl ring of Y391 of GsaCT and R131^{3.50} or (F) between the carbonyl oxygen of C347 of GtaCT and R135^{3.50}. Gray bars indicate the range of mobility of GsCT in MD simulations of the X-ray structures of (left) holo $\beta_2AR^* \cdot Gs^{empty}$ (taken from ref. [25]) or (right) RhR*•GtaCT (see Figs B, C and E in S1 File; see Methods section). The mobility of switched GsaCT (after about 100 ns) is only slightly increased, when compared to the mobility of the corresponding section in $\beta_2AR^* \cdot Gs^{empty}$ (grey). The time series data are drawn on top of the raw data as a running average. The plots are linear for the first 10 ns and logarithmic for the remaining time (gray dashed lines). The four representative simulations (black, red, blue, green) of 11-mer GsaCT (Panel A of Fig N in S1 File, simulations 8, 9, 21 and 23) and of 11-mer GtaCT (Panel B of Fig N in S1 File, simulations 9, 16, 21 and 30) were picked from 8 and 10 simulations where a helix-switch was observed (Fig N in S1 File).

doi:10.1371/journal.pone.0143399.g003

terminal reverse turn and the ICL3 are completely structured in our models of R*•G^{GDP} intermediates. These intermediates already show a “double sandwich” structure comprising—in that order—the $\alpha N/\beta 2\text{-}\beta 3$ loop of α , ICL2 of R*, $\alpha 5$ helix of α , and ICL3 of R* (Fig 2A, for GtaCT see [14]). This “sandwich” is also seen in the $\beta_2AR^* \cdot Gs^{empty}$ complex. In contrast to the $\beta_2AR^* \cdot Gs^{empty}$ complex, however, $\alpha 5$ is not displaced in the intermediates. We conclude that the interaction of the structural elements within the “double sandwich” structure generate a structural framework for the $\alpha 5$ helix-switch, which, according to our model, is guided by different sets of interactions with the cytoplasmic crevice of R*. However, we do not exclude that, in addition to $\alpha 5$, interactions of other elements of that structural framework, such as the $\alpha N/$

$\beta 2$ - $\beta 3$ loop of $G\alpha$ with ICL2 of R^* , are involved in coupling of the R^* interface with the nucleotide binding pocket.

The existence of the $R^* \cdot G^{GDP}$ intermediate, in which GDP is still bound in the nucleotide binding site of the $G\alpha$ subunit, was first derived from the kinetics of Gt activation in disc membrane [13,14] and HDX experiments of Gs binding to β_2AR^* [15]. In the latter work, Sunahara and co-workers provided first evidence for GDP bound $G\alpha$ which couples to β_2AR^* mainly through $G\alpha CT$. In the present analysis of the intermediate complex, $G\alpha CT$ is bound to β_2AR^* through a strong hydrogen bond between E392 and R131^{3,50} of TM3 employing the E(D)RY motif. Additional hydrogen bonds are formed from $G\alpha CT$ to ICL2 and 3 (Fig 2A–2C). Interactions with ICL2 are in line with previous work [28], where mutations of the ICL2 of rhodopsin lead to a receptor that binds but does not activate G protein, thus likely stabilizing an $R^* \cdot G^{GDP}$ intermediate [29].

In the intermediate state models of both RhR^* and β_2AR^* , neither $G\alpha CT$ nor $G\alpha CT$ exhibit extended hydrophobic interactions. The presence of transient polar interactions and the absence of stable hydrophobic interactions is indicative of intermediate states, as the full desolvation potential is not yet exploited [27]. In the context of receptor G protein coupling, it specifically reflects the weak binding of G^{GDP} to the receptor. In agreement with these characteristic properties, $G\alpha CT$ in the intermediate position is highly dynamic in the MD simulations. The peptides either unfold and diffuse away or switch to the position of the nucleotide free complex within nanoseconds (Fig 2). Taking into consideration that the simulations were performed with the peptides and not with the holo G protein, it is likely that the switch of the $\alpha 5$ helix, which would be constrained by additional contacts with G^{GDP} , occurs at considerably longer timescales. This assumption would be in line with the estimated microsecond lifetimes for intermediary states by the Frauenfelder model of protein dynamics [30].

Intrinsic switching of the $\alpha 5$ helix at the R^* interface

The two binding modes obtained from flexible docking analysis of $G\alpha CT$ to R^* were assigned to the GDP bound and nucleotide free $R^* \cdot G$ states. Comparison of these successive states indicates that the $\alpha 5$ helix-switching motion is promoted by consecutive interactions with the cytoplasmic crevice of R^* . Further, MD simulations started from the putative GDP bound complexes show that this mechanism is structurally realizable, because the peptides very rapidly switch to adopt the stable position of the nucleotide free state. All key interactions present in the X-ray structures are eventually restored (Fig 3). This is not only seen for $RhR^* \cdot G\alpha CT$, for which an X-ray structure of R^* with 11-mer $G\alpha CT$ exists [5,31] but also for $\beta_2AR^* \cdot G\alpha CT$, where additional contacts of Gs with β_2AR^* conceivably co-determine the position of $\alpha 5$ [3]. Thus, in principle no additional forces or constraints are required for $G\alpha CT$ and $G\alpha CT$ for transition from their intermediate states to the position and orientation they have in the nucleotide free states. Specifically, the only apparent forces are the interactions of the far C-terminus of $\alpha 5$ with the cytoplasmic crevice of R^* and the expulsion of solvent. Thus, we argue that the ability of the $\alpha 5$ helix to switch is an intrinsic feature of the coupling interface comprising $G\alpha CT$ and the cytoplasmic crevice of R^* . Following the theory of complex formation [27], transition from intermediates to the final functional states is guided by a reorganization of electrostatic interactions and dewetting of the interaction interfaces. In agreement with this notion, we observe new hydrogen bonds (Fig 2A–2D and Fig O in S1 File), expulsion of water, and formation of an extended hydrophobic contact patch at the binding interface of $G\alpha CT$ and ICL3 of R^* (Figs K, Q and R in S1 File).

Formation of these new interactions presumably lowers the free energy required to reach the transition state, in which the contacts with the $\beta 2$, $\beta 3$, $\beta 5$ and $\beta 6$ half-barrel of G^{GDP} and

the interaction with GDP, which lock $\alpha 5$ in its inactive position, are broken. At this specific point, our simulations complement recent microsecond MD simulations, where receptor-mimicking restraints led to displacement of $\alpha 5$ in GDP bound $G\alpha$ [10]. While harmonic position restraints were applied in the former analysis to guide interface atoms of $G\alpha$ (and thereby $\alpha 5$) to the positions of corresponding atoms in the $\beta_2AR^* \cdot Gs^{empty}$ crystal structure, our unbiased MD simulations explicitly reveal the reorganisation of contacts with R^* that promote displacement of $\alpha 5$. Unlocking $\alpha 5$ from its inactive position results in a progressive downhill reaction, which includes displacement of the helical domain, disordering of the $\beta 1$ - $\alpha 5$ loop, breakage of the interactions stabilizing GDP and formation of new contacts between $\alpha 5$ and the $G\alpha$ half barrel. Taken together, we conclude that the interactions of $\alpha 5$ with the R^* interface are the key driving forces for its switching motion, which ultimately leads to GDP release.

The $\alpha 5$ helix-switch involves highly conserved structural elements

In the mechanism proposed here, the $\alpha 5$ helix acts as a lever arm that transmits the signal from R^* to the GDP binding pocket. The $\alpha 5$ helix thereby inherently exposes two adjacent sites to highly conserved motifs at $R^{3.50}$ and at the $P^{3.57}$ cap motif of TM3 (Fig 2, Fig I in S1 File and Table A in S1 File). Thus, two different (but not mutually distinct) interaction networks are sequentially engaged during the transition from $R^* \cdot G^{GDP}$ to the $R^* \cdot G^{empty}$ complex. Conceivably, these interaction networks could have a role for receptor G protein coupling specificity, when $R^* / G\alpha$ C-terminus complementarity is verified twice. The interaction network for $R^* \cdot G^{GDP}$ would not require altering the position of $\alpha 5$ and would consequently be uncoupled from GDP release. Such a scenario is in line with the formation of a non-productive pre-coupled complex and with a role of the $G\alpha$ C-terminus in controlling the kinetics and specificity of GPCR signalling pathways [16,17]. Indeed, the observed interaction between $R131^{3.50}$ and the carboxyl group of E392 in the $\beta_2AR^* \cdot G^{GDP}$ complex would explain the key role of E392 in selective activation of Gs [32], because no contacts with its acidic side chain are observed in the X-ray structure of the $\beta_2AR^* \cdot Gs^{empty}$ complex. More generally, the involvement of the highly conserved motifs at $R^{3.50}$ and at the $P^{3.57}$ cap motif of TM3 (Fig S in S1 File; Panel A of Figs P and Q in S1 File; Table A in S1 File) in the hydrogen bond network between $G\alpha CT$ and R^* indicates that the observed mechanism may apply in similar form to other GPCR/G protein systems.

Conclusion

As the first specific complex during receptor-catalyzed nucleotide exchange, the $R^* \cdot G^{GDP}$ intermediate pre-complex provides a structural framework, in which the $\alpha 5$ helix can act as a rod to transmit the signal from the activated receptor R^* to the GDP binding pocket in the G protein α -subunit. Our simulations reveal the dynamic interactions which occur during the “helix-switch”. It is found that, starting from $R^* \cdot G^{GDP}$, the C-terminal end of $\alpha 5$ undergoes a characteristic screw-like motion and reconstitutes all specific contacts of the nucleotide free $R^* \cdot G^{empty}$ complex spontaneously and without external interaction. We conclude that the interactions of $\alpha 5$ with R^* in the $R^* \cdot G^{GDP}$ complex initiate a progressive downhill reaction which ultimately leads to GDP release.

Methods

Structure preparation

The structural models underlying the docking experiments and the MD simulations were prepared based on X-ray structures from co-crystals of β_2AR^* with $G\alpha\beta\gamma$ [3] and of RhR^* with

Gt α CT [5]. The Gt α CT binding cavities in the crystal structures of Ops*/ Meta II with (PDB entry 3DQB/ 3PQR) and without (PDB entry 3CAP/ 3PXO) Gt α CT do not differ significantly from each other in backbone RMSD. We selected 3DQB as a representative of the active Meta II state of rhodopsin (termed RhR*). For all simulations involving β_2 AR*, the coordinates from the β_2 AR*•Gs^{empty} complex (PDB entry 3SN6) with the agonist bound but with the T4-lysozyme removed from the N-terminus, were used. To prepare the complex for simulation, unresolved side chain atoms were added and three mutated residues (M96T, M98T and N187E) in β_2 AR* were changed back to the wild-type form. The coordinates for the missing residues of ECL 2 (176–178) were taken from the nanobody-stabilized active β_2 AR*-structure (PDB entry 3P0G). The conformation of the residues 240 to 264 from ICL 3, which are not critical to receptor function [33], were modelled with help of the loop modeling program SuperLooper [34]. Of note, none of the modelled sections were part of the cytoplasmic crevice. Internal water molecules were added as described in the Protocol B of [S1 File](#) as well as the choice of appropriate protonation states.

Flexible docking analysis

We applied the flexible docking protocol from our previous analysis, with fixed main chain but flexible side chain topologies of R* and G α CT. This allowed fast calculation of a large conformational space of possible G α CT binding modes and conformations while staying close to experimentally determined structures. Flexible docking analysis of β_2 AR* and 15-mer G α CT was performed with the program GOLD as described previously [14]. The docking program GOLD [35] is based on a genetic algorithm to explore a defined range of ligand conformational flexibility with partial flexibility of the receptor. The docking results of β_2 AR* and 15-mer G α CT from 11 independent runs were clustered applying the single linkage method with a cut-off of 1.5 Å as implemented in the tool `g_cluster` of the program GROMACS (see Protocol C in [S1 File](#) for more information).

Molecular dynamics simulations

We performed unbiased all-atom MD simulations of β_2 AR*/ RhR* and 11/19-mer G α CT with explicit water molecules and a lipid bilayer. The peptide length was derived from analysis of simulations of β_2 AR*•Gs / G α CT complexes, which revealed that the binding interface with $\alpha 5$ maximally consists of 15 C-terminal residues [25]. Simulations were carried out with 11-mer peptides, reassembling the length of Gt α CT used in binding assays and for X-ray crystallography and with 19-mer peptides, where the helicity of the 15-mer is preserved through hydrogen bonding with the N-terminal extension.

System preparation and subsequent minimization and equilibration were performed with the GROMACS suite (version 4.5) [36]. The prepared proteins (see Protocol A of [S1 File](#)) were inserted into the equilibrated bilayer of dimyristoylphosphatidylcholine (DMPC) using the GROMACS `g_membed` tool [37]. Parameters for the DMPC lipids were derived from Berger et al. [38] and for water from the SPC/E model [39]. A salt concentration of 0.15 mol/L was obtained by adding Na⁺ and Cl⁻ ions to the system with the GROMACS tool `genion`. The AMBER99SB-ILDN force field [40] was used for proteins and ions. Ligand parameters for the agonist *5-hydroxy-4H-benzo[1,4]oxazin-3-one* of β_2 AR* were created with the PRODRG2 web-server [41].

The simulation protocol consisting of energy minimization, equilibration and production runs was performed as described in Protocol D of [S1 File](#). The MD simulations starting with G α CT from the position and orientation of the co-crystals consist of ten 200 ns MD runs for RhR*•Gt α CT and β_2 AR*•G α CT, respectively [25]. The 30 simulations starting from the

respective complexes in the putative $R^* \cdot G^{GDP}$ intermediate were 100 ns long for the RhR*/Gt α CT system and 200 ns for the β_2 AR*/G α CT system.

Supporting Information

S1 File. Includes Protocols A-G, Table A and Figures A-S.
(PDF)

Acknowledgments

This work was supported by the Deutsche Forschungsgemeinschaft Sfb740 (to K.P.H., P.S. and P.W.H.), Sfb1078-B6 (to P.S.), DFG HI 1502/1-1 (to P.W.H.), BI 893/8 (to P.W.H.), DFG Cluster of Excellence ‘Unifying Concepts in Catalysis’ (Research Field D3/E3-1 to P.S.) and ERC Advanced grant (ERC-2009/249910—TUDOR to K.P.H.). The computer time necessary for this project was provided in part by the “Norddeutscher Verbund für Hoch und Höchstleistungsrechner” (HLRN). U.Z. acknowledges funding from the Scottish Universities Physics Alliance and the UK National Physical Laboratory.

Author Contributions

Conceived and designed the experiments: ASR PWH. Performed the experiments: ASR PWH. Analyzed the data: ASR PWH. Contributed reagents/materials/analysis tools: ASR UZ HG PWH. Wrote the paper: ASR UZ HG KPH PS PWH.

References

1. Katritch V, Cherezov V, Stevens RC. Diversity and modularity of G protein-coupled receptor structures. *Trends Pharmacol Sci*. Elsevier Ltd; 2012; 33: 17–27. doi: [10.1016/j.tips.2011.09.003](https://doi.org/10.1016/j.tips.2011.09.003)
2. Oldham WM, Hamm HE. Heterotrimeric G protein activation by G-protein-coupled receptors. *Nat Rev Mol Cell Biol*. 2008; 9: 60–71. doi: [10.1038/nrm2299](https://doi.org/10.1038/nrm2299) PMID: [18043707](https://pubmed.ncbi.nlm.nih.gov/18043707/)
3. Rasmussen SGF, DeVree BT, Zou Y, Kruse AC, Chung KY, Kobilka TS, et al. Crystal structure of the β_2 adrenergic receptor-Gs protein complex. *Nature*. 2011/07/21 ed. 2011; 477: 549–55. doi: [10.1038/nature10361](https://doi.org/10.1038/nature10361) PMID: [21772288](https://pubmed.ncbi.nlm.nih.gov/21772288/)
4. Farrens DL, Altenbach C, Yang K, Hubbell WL, Khorana HG. Requirement of rigid-body motion of transmembrane helices for light activation of rhodopsin. *Science* (80-). Department of Biology, Massachusetts Institute of Technology, Cambridge, MA 02139, USA.; 1996; 274: 768–770. Available: <http://www.ncbi.nlm.nih.gov/pubmed/8864113>
5. Scheerer P, Park JH, Hildebrand PW, Kim YJ, Krauss N, Choe H-W, et al. Crystal structure of opsin in its G-protein-interacting conformation. *Nature*. Institut für Medizinische Physik und Biophysik (CC2), Charité—Universitätsmedizin Berlin, Charitéplatz 1, D-10117 Berlin, Germany.: Nature Publishing Group; 2008; 455: 497–502. Available: <http://www.nature.com/nature/journal/v455/n7212/abs/nature07330.html>
6. Kruse AC, Ring AM, Manglik A, Hu J, Hu K, Eitel K, et al. Activation and allosteric modulation of a muscarinic acetylcholine receptor. *Nature*. Nature Publishing Group; 2013; 504: 101–6. doi: [10.1038/nature12735](https://doi.org/10.1038/nature12735)
7. Wall MA, Coleman DE, Lee E, Iñiguez-Lluhi JA, Posner BA, Gilman AG, et al. The structure of the G protein heterotrimer G α 1 β 1 γ 2. *Cell*. 1995; 83: 1047–1058.
8. Hofmann KP, Scheerer P, Hildebrand PW, Choe H-W, Park JH, Heck M, et al. A G protein-coupled receptor at work: the rhodopsin model. *Trends Biochem Sci*. Institut für Medizinische Physik und Biophysik (CC2), Charité—Universitätsmedizin Berlin, Charitéplatz 1, D-10117 Berlin, Germany. klaus_p-eter.hofmann@charite.de; 2009; 34: 540–52. doi: [10.1016/j.tibs.2009.07.005](https://doi.org/10.1016/j.tibs.2009.07.005)
9. Rasmussen SGF, Devree BT, Zou Y, Kruse AC, Chung KY, Kobilka TS, et al. Crystal structure of the β (2) adrenergic receptor-Gs protein complex. *Nature*. 1] Department of Molecular and Cellular Physiology, Stanford University School of Medicine, Stanford, California 94305, USA [2] , 2200 Copenhagen N, Denmark [3].: Nature Publishing Group; 2011; 450: 383–387. Available: <http://eutils.ncbi.nlm.nih.gov/entrez/eutils/elink.fcgi?dbfrom = pubmed&id=21772288&retmode = ref&cmd = prlinks>

10. Dror RO, Mildorf TJ, Hilger D, Manglik A, Borhani DW, Arlow DH, et al. Structural basis for nucleotide exchange in heterotrimeric G proteins. *Science* (80-). 2015; 348: 1361–1365. doi: [10.1126/science.aaa5264](https://doi.org/10.1126/science.aaa5264)
11. Shim J-Y, Ahn KH, Kendall D a. Molecular basis of cannabinoid CB1 receptor coupling to the G protein heterotrimer Gaiβγ: identification of key CB1 contacts with the C-terminal helix α5 of Gai. *J Biol Chem*. 2013; 288: 32449–65. doi: [10.1074/jbc.M113.489153](https://doi.org/10.1074/jbc.M113.489153) PMID: [24092756](https://pubmed.ncbi.nlm.nih.gov/24092756/)
12. Mnpotra JS, Qiao Z, Cai J, Lynch DL, Grossfield A, Leioatts N, et al. Structural Basis of G Protein-Coupled Receptor- Gi Protein Interaction: Formation of the Cannabinoid CB2 Receptor / Gi Protein Complex. *J Biol Chem*. 2014; 0–31. doi: [10.1074/jbc.M113.539916](https://doi.org/10.1074/jbc.M113.539916)
13. Heck M, Hofmann KP. Maximal rate and nucleotide dependence of rhodopsin-catalyzed transducin activation: initial rate analysis based on a double displacement mechanism. *J Biol Chem*. 2001; 276: 10000–9. doi: [10.1074/jbc.M009475200](https://doi.org/10.1074/jbc.M009475200) PMID: [11116153](https://pubmed.ncbi.nlm.nih.gov/11116153/)
14. Scheerer P, Heck M, Goede A, Park J, Choe H, Ernst OP, et al. Structural and kinetic modeling of an activating helix switch in the rhodopsin-transducin interface. *Proc Natl Acad Sci U S A. Institut für Medizinische Physik und Biophysik (CC2) and.*; 2009; 106: 10660–10665. Available: <http://www.pnas.org/content/106/26/10660.abstract>
15. Chung KY, Rasmussen SGF, Liu T, Li S, Devree BT, Chae PS, et al. Conformational changes in the G protein Gs induced by the β2 adrenergic receptor. *Nature*. Nature Publishing Group; 2011; 477: 611–615. Available: <http://www.nature.com/doi/10.1038/nature10488>
16. Damian M, Mary S, Maingot M, M'Kadmi C, Gagne D, Leyris J-P, et al. Ghrelin receptor conformational dynamics regulate the transition from a preassembled to an active receptor:Gq complex. *Proc Natl Acad Sci*. 2015; 112: 1601–1606. doi: [10.1073/pnas.1414618112](https://doi.org/10.1073/pnas.1414618112) PMID: [25605885](https://pubmed.ncbi.nlm.nih.gov/25605885/)
17. Ayoub MA, Trinquet E, Pflieger KDG, Pin J-P. Differential association modes of the thrombin receptor PAR1 with Galphai1, Alpha12, and beta-arrestin 1. *FASEB J*. 2010; 24: 3522–3535. doi: [10.1096/fj.10-154997](https://doi.org/10.1096/fj.10-154997) PMID: [20410441](https://pubmed.ncbi.nlm.nih.gov/20410441/)
18. Kisselev OG, Kao J, Ponder JW, Fann YC, Gautam N, Marshall GR. Light-activated rhodopsin induces structural binding motif in G protein alpha subunit. *Proc Natl Acad Sci U S A. Institute for Biomedical Computing, Washington University Medical School, St. Louis, MO 63110, USA.*; 1998; 95: 4270–4275. Available: <http://eutils.ncbi.nlm.nih.gov/entrez/eutils/efetch.fcgi?dbfrom=pubmed&id=9539726&retmode=ref&cmd=prlinks>
19. Koenig BW, Kontaxis G, Mitchell DC, Louis JM, Litman BJ, Bax A. Structure and orientation of a G protein fragment in the receptor bound state from residual dipolar couplings. *J Mol Biol*. 2002/09/10 ed. 2002; 322: 441–461. S0022283602007453 [pii] PMID: [12217702](https://pubmed.ncbi.nlm.nih.gov/12217702/)
20. Choe H- W, Kim YJ, Park JH, Morizumi T, Pai EF, Krauss N, et al. Crystal structure of metarhodopsin II. *Nature*. Nature Publishing Group, a division of Macmillan Publishers Limited. All Rights Reserved.; 2011; 471: 651–5.
21. Deupi X, Edwards P, Singhal A, Nickle B, Oprian D, Schertler G, et al. Stabilized G protein binding site in the structure of constitutively active metarhodopsin-II. *Proc Natl Acad Sci U S A. Paul Scherrer Institut, Villigen PSI, 5232, Switzerland.*; 2012; 109: 119–24. Available: <http://www.pnas.org/cgi/content/abstract/109/1/119>
22. Standfuss J, Edwards PC, D'Antona A, Fransen M, Xie G, Oprian DD, et al. The structural basis of agonist-induced activation in constitutively active rhodopsin. *Nature*. 2011; 471: 656–60.
23. Kim TH, Chung KY, Manglik A, Hansen AL, Dror RO, Mildorf TJ, et al. The Role of Ligands on the Equilibria Between Functional States of a. *J Am Chem Soc. American Chemical Society*; 2013; 135: 9465–74. doi: [10.1021/ja404305k](https://doi.org/10.1021/ja404305k)
24. Elgeti M, Rose AS, Bartl FJ, Hildebrand PW, Hofmann K-P, Heck M. Precision vs flexibility in GPCR signaling. *J Am Chem Soc*. 2013; 135: 12305–12. doi: [10.1021/ja405133k](https://doi.org/10.1021/ja405133k) PMID: [23883288](https://pubmed.ncbi.nlm.nih.gov/23883288/)
25. Rose AS, Elgeti M, Zachariae U, Grubmüller H, Hofmann KP, Scheerer P, et al. Position of transmembrane helix 6 determines receptor g protein coupling specificity. *J Am Chem Soc*. 2014; 136: 11244–7. doi: [10.1021/ja5055109](https://doi.org/10.1021/ja5055109) PMID: [25046433](https://pubmed.ncbi.nlm.nih.gov/25046433/)
26. Alexander NS, Preininger AM, Kaya AI, Stein RA, Hamm HE, Meiler J. Energetic analysis of the rhodopsin-G-protein complex links the α5 helix to GDP release. *Nat Struct Mol Biol*. 2014; 21: 56–63. doi: [10.1038/nsmb.2705](https://doi.org/10.1038/nsmb.2705) PMID: [24292645](https://pubmed.ncbi.nlm.nih.gov/24292645/)
27. Schreiber G. Kinetic studies of protein-protein interactions. *Curr Opin Struct Biol*. 2002; 12: 41–7. Available: <http://www.ncbi.nlm.nih.gov/pubmed/11839488> PMID: [11839488](https://pubmed.ncbi.nlm.nih.gov/11839488/)
28. Franke R, König B, Sakmar T, Khorana H, Hofmann K. Rhodopsin mutants that bind but fail to activate transducin. *Science* (80-). Department of Biology, Massachusetts Institute of Technology, Cambridge 02139.; 1990; 250: 123–125. doi: [10.1126/science.2218504](https://doi.org/10.1126/science.2218504)

29. Ernst OP, Hofmann KP, Sakmar TP. Characterization of rhodopsin mutants that bind transducin but fail to induce GTP nucleotide uptake. Classification of mutant pigments by fluorescence, nucleotide release, and flash-induced light-scattering assays. *J Biol Chem*. Howard Hughes Medical Institute, Laboratory of Molecular Biology and Biochemistry, Rockefeller University, New York, New York 10021, USA.; 1995; 270: 10580–10586. Available: <http://eutils.ncbi.nlm.nih.gov/entrez/eutils/elink.fcgi?dbfrom=pubmed&id=7737995&retmode=ref&cmd=prlinks>
30. Frauenfelder H, Sligar S, Wolynes P. The energy landscapes and motions of proteins. *Science* (80-). 1991; 254: 1598–1603. doi: [10.1126/science.1749933](https://doi.org/10.1126/science.1749933)
31. Park JH, Scheerer P, Hofmann KP, Choe H-W, Ernst OP. Crystal structure of the ligand-free G-protein-coupled receptor opsin. *Nature*. Institut für Medizinische Physik und Biophysik (CC2), Charité-Universitätsmedizin Berlin, Charitéplatz 1, D-10117 Berlin, Germany.; Nature Publishing Group; 2008; 454: 183–187. Available: <http://www.nature.com/nature/journal/v454/n7201/abs/nature07063.html>
32. Natochin M, Muradov KG, McEntaffer RL, Artemyev NO. Rhodopsin Recognition by Mutant Gs Containing C-terminal Residues of Transducin. *J Biol Chem*. 2000; 275: 2669–2675. doi: [10.1074/jbc.275.4.2669](https://doi.org/10.1074/jbc.275.4.2669) PMID: [10644728](https://pubmed.ncbi.nlm.nih.gov/10644728/)
33. Rubenstein RC, Wong SK, Ross EM. The hydrophobic tryptic core of the beta-adrenergic receptor retains Gs regulatory activity in response to agonists and thiols. *J Biol Chem*. 1987; 262: 16655–16662. Available: <http://www.jbc.org/cgi/content/abstract/262/34/16655> PMID: [2890639](https://pubmed.ncbi.nlm.nih.gov/2890639/)
34. Hildebrand PW, Goede A, Bauer RA, Gruening B, Ismer J, Michalsky E, et al. SuperLooper—a prediction server for the modeling of loops in globular and membrane proteins. *Nucleic Acids Res*. Institute of Medical Physics and Biophysics, Charité, University of Medicine, Berlin, Germany. peter.hildebrand@charite.de; Oxford University Press; 2009; 37: W571–4. doi: [10.1093/nar/gkp338](https://doi.org/10.1093/nar/gkp338)
35. Verdonk ML, Cole JC, Hartshorn MJ, Murray CW, Taylor RD. Improved protein-ligand docking using GOLD. *Proteins*. 2003; 52: 609–23. Available: <http://www.ncbi.nlm.nih.gov/pubmed/12910460> PMID: [12910460](https://pubmed.ncbi.nlm.nih.gov/12910460/)
36. Hess B, Kutzner C, van der Spoel D, Lindahl E. GROMACS 4: Algorithms for Highly Efficient, Load-Balanced, and Scalable Molecular Simulation. *J Chem Theory Comput*. American Chemical Society; 2008; 4: 435–447.
37. Wolf MG, Hoefling M, Aponte-Santamaría C, Grubmüller H, Groenhof G. g_membed: Efficient insertion of a membrane protein into an equilibrated lipid bilayer with minimal perturbation. *J Comput Chem*. 2010; 31: 2169–74. doi: [10.1002/jcc.21507](https://doi.org/10.1002/jcc.21507) PMID: [20336801](https://pubmed.ncbi.nlm.nih.gov/20336801/)
38. Berger O, Edholm O. Molecular dynamics simulations of a fluid bilayer of dipalmitoylphosphatidylcholine at full hydration, constant pressure, and constant temperature. *Biophys J*. 1997; 72: 2002–2013. Available: <http://www.sciencedirect.com/science/article/pii/S0006349597788453> PMID: [9129804](https://pubmed.ncbi.nlm.nih.gov/9129804/)
39. Berendsen HJC, Grigera JR, Straatsma TP. The Missing Term in Effective Pair Potentials. *J Phys Chem*. Inst Fis Liquidos & Sistemas Biol, Ra-1900 La Plata, Argentina; 1987; 91: 6269–6271. Available: <http://links.isiglobalnet2.com/gateway/Gateway.cgi?GWVersion=2&SrcAuth=mekentosj&SrcApp=Papers&DestLinkType=FullRecord&DestApp=WOS&KeyUT=A1987K994100038>
40. Lindorff-Larsen K, Piana S, Palmo K, Maragakis P, Klepeis JL, Dror RO, et al. Improved side-chain torsion potentials for the Amber ff99SB protein force field. *Proteins*. D. E. Shaw Research, New York, New York 10036, USA.; 2010; 78: 1950–1958. Available: http://sfx.mpg.de/sfx_local?id=doi:10.1002/prot.22711
41. Schüttelkopf AW, van Aalten DMF. PRODRG: a tool for high-throughput crystallography of protein-ligand complexes. *Acta Crystallogr D Biol Crystallogr*. Division of Biological Chemistry and Molecular Microbiology, Wellcome Trust Biocentre, School of Life Sciences, University of Dundee, Dow Street, DD1 5EH, Scotland.; 2004; 60: 1355–63. doi: [10.1107/S0907444904011679](https://doi.org/10.1107/S0907444904011679)